APPLIED SCIENCES AND ENGINEERING

An ICU-grade breathable cardiac electronic skin for health, diagnostics, and intraoperative and postoperative monitoring

Qiuna Zhuang[1]†, Kuanming Yao[2]†, Xian Song[1], Qiang Zhang[2], Chi Zhang[1], Huiming Wang[1], Ruofan Yang[1], Guangyao Zhao[2], Shanghang Li[3], Haihua Shu[3], Qiyao Huang[4,5], Yunfei Chai[3]*, Xinge Yu[2,6,7,8]*, Zijian Zheng[1,4,9,10,11]*

Cardiovascular digital health technologies potentially outperform traditional clinical equipment through their noninvasive, on-body, and portable monitoring with mass cardiac data beyond the confines of inpatient settings. However, existing cardiovascular wearables have difficulty with providing medical-grade accuracy with a chronically comfortable and stable patient/consumer device interface for reliable clinical decision-making. Here, we develop an intensive care unit (ICU)–grade breathable cardiac electronic skin system (BreaCARES) for real-time, wireless, continuous, and comfortable cardiac care. BreaCARES enables a novel digital cardiac care platform for health care, outpatient diagnostics, stable intraoperative monitoring during heart surgery, and continuous and comfortable inpatient postoperative cardiac care, exhibiting ICU-grade accuracy while having superior anti-interference stability, portability, and long-term on-skin biocompatibility to the clinically and commercially available cardiac monitors in cardiovascular ICUs.

INTRODUCTION

Cardiovascular diseases, the top leading cause of global death (*1*), take an estimate of 18 million people's lives annually. Long-term continuous monitoring of cardiac signals is crucial for the assessment of cardiovascular health (*2*, *3*), detection of acute cardiac dysfunction (*4*), and the implementation of timely medical treatment (*5*).

Electrocardiogram (ECG) is the most widely accepted clinical cardiovascular monitoring standard (*6*–*8*), as it provides comprehensive information for detecting cardiac abnormalities in heart diseases [e.g., arrhythmias, myocardial infarction (MI), and heart failure symptoms], chronic diseases (e.g., diabetes and HIV infection), and sudden cardiac arrest (*7*) and remains a cornerstone for continuous monitoring in intensive care units (ICUs) (*9*). However, current clinical devices and systems are usually multiple hard wired, specialist required, invasive, and cumbersome. Alternatively, digital health technologies based on soft and wearable electronic materials (*10*–*14*), devices (*15*–*17*), and systems (*18*–*25*) potentially enable noninvasive, on-body, and portable health care monitoring (*26*–*30*) for at-risk individuals beyond the confines of clinical inpatient settings.

Nevertheless, existing wearable technologies suffer from unaddressed gaps in clinical translations and adoptions (*31*–*33*), and the achievement of ICU-grade accuracy is rare (*20*, *21*, *34*). The "ICU-grade accuracy" refers to the high level of precision and reliability comparable with standard clinically proven machines in ICU settings, particularly in early diagnosis, and continuous tracking of vital signs among critically ill patients. The successful implementation of wearable devices/systems with medical-grade accuracy in ICUs is critical yet challenging. These ongoing challenges include the following: (i) difficulties in achieving medical-grade accuracy with real-time and sufficient datasets for reliable clinical decision-making because of instable and noisy biointerfaces along with the lack of complex system-level integration; (ii) poor patient/consumer compliance owing to skin intolerance of uncomfortable monitoring devices with bulky form factors and impermeable gel electrodes over long-term wear; (iii) compounding risks of potential injury on fragile skin with possible dermatological comorbidities among elderly, neonates, and seriously ill patients, especially in ICUs.

Here, we develop a wireless, fully integrated, and breathable cardiac electronic skin system (BreaCARES) in a thin, lightweight, skin-like soft, and permeable design form factor for continuous and comfortable cardiac care. We demonstrate the versatility of this cardiac platform on animal models, healthy volunteers (Fig. 1A), anti-interference stable intraoperative monitoring of surgical patients (Fig. 1B), and ICU-grade postoperative cardiac care with superior biocompatibility and comfort (Fig. 1, C and D) to the clinical counterpart (Fig. 1, C and E). BreaCARES is composed of multilayer-patterned, permeable, and stretchable liquid metal (LM) microcircuits, which three-dimensionally integrate with electronic components in high density. Eutectic gallium-based LM leverages outstanding biocompatibility (*35*–*38*), softness (*39*), configurability (*40*, *41*), stretchability, and conductivity (*2*, *42*, *43*). BreaCARES has a low-impedance, wet-adhesive, and biofriendly user-system interface, enabling a continuous and stable biointerface with high signal quality in various daily and clinical activities while preventing any skin erythema or inflammation over week-long attachment. The whole system is as thin as 180 μm (Fig. 1F) and is only 0.489 g

---

[1]Laboratory for Advanced Interfacial Materials and Devices, Department of Applied Biology and Chemical Technology, Hong Kong Polytechnic University, Hong Kong SAR, China. [2]Department of Biomedical Engineering, City University of Hong Kong, Hong Kong SAR, China. [3]Anesthesiology Department of Guangdong Cardiovascular Institute, Guangdong Provincial People's Hospital, Southern Medical University, Guangzhou, China. [4]Research Institute for Intelligent Wearable Systems (RI-IWEAR), Hong Kong Polytechnic University, Hong Kong SAR, China. [5]School of Fashion and Textiles, Hong Kong Polytechnic University, Hong Kong SAR, China. [6]Hong Kong Centre for Cerebro-Cardiovascular Health Engineering (COCHE), Hong Kong Science Park, Hong Kong SAR, China. [7]Hong Kong Institute for Clean Energy, City University of Hong Kong, Hong Kong SAR, China. [8]Institute of Digital Medicine, City University of Hong Kong, Hong Kong SAR, China. [9]Research Institute for Smart Energy (RISE), Hong Kong Polytechnic University, Hong Kong SAR, China. [10]Soft Electronics Research Centre, PolyU-Wenzhou Technology and Innovation Research Institute, Wenzhou, Zhejiang Province, China. [11]PolyU-Daya Bay Technology and Innovation Research Institute, Huizhou, Guangdong Province, China.
*Corresponding author. Email: tczzheng@polyu.edu.hk (Z.Z); xingeyu@cityu.edu.hk (X.Y); wochaiyunfei@163.com (Y.C.)
†These authors contributed equally to this work.

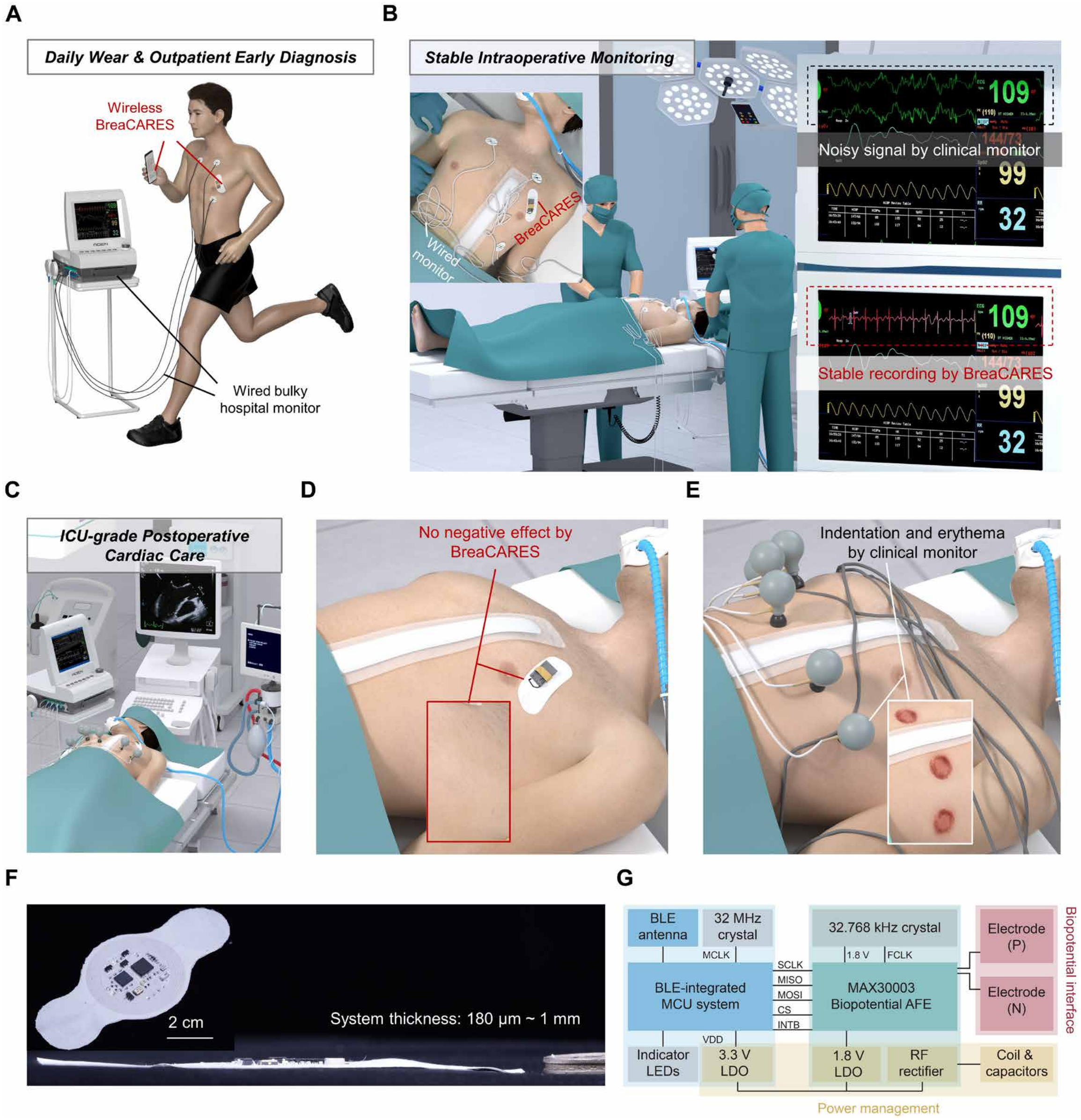

Fig. 1. BreaCARES for ICU-grade wireless, stable, continuous, and comfortable health care, outpatient diagnostics, intraoperative monitoring, and postoperative cardiac care. (**A**) Schematic illustration showing the monolithically integrated BreaCARES with a conformal and comfortable biointerface for wireless and real-time cardiac care through a portable device (e.g., a smartphone with a customized mobile app), while the conventional clinical monitor is multiple wired and bulky. (**B** and **C**) Schematic illustration showing the BreaCARES in intraoperative cardiac monitoring of surgical patients and ICU-grade postoperative cardiac care, respectively. (**D** and **E**) Skin surface status of an ICU patient after using BreaCARES and clinical monitor, respectively. (**F**) Digital images showing thin, soft, and high-integration-density BreaCARES. (**G**) Block diagram of BreaCARES consisting of electrodes, a biopotential sensing chip as the AFE for ECG sampling (sampling rate: 500 Hz), 1.8-V LDO and a 32.768-kHz crystal for driving the sampling of AFE, and a BLE-integrated MCU for wireless data acquisition, transmission, and functional control.

in weight (fig. S1), allowing the acquisition, analysis, and transmission of cardiac data in a wireless and real-time manner (Fig. 1G).

RESULTS

Structure and properties of BreaCARES

As shown in Fig. 2A, the cardiac system typically consisted of five stretchable and permeable layers including (i) a bioadhesive hydrogel mat, (ii) a pair of LM biopotential electrodes embedded in the base layer of an LM three-dimensional (3D) circuit, (ii) an upper layer of the LM 3D circuit, (iv) a paste mask layer bonded with electronic components (labeled in Fig. 2B) by a stretchable hybrid LM solder, and (v) an encapsulation layer made of the permeable but waterproof fiber mat. The microporous fibrous structure of the electrospun fiber mat allows air and moisture (water vapor) to pass through it, while the intrinsic hydrophobicity of the poly(styrene-*block*-butadiene-*block*-styrene) (SBS) fiber mat can repel water droplets. Therefore, permeability and waterproofness are achieved at the same time. The detailed fabrication protocol is illustrated in Materials and Methods.

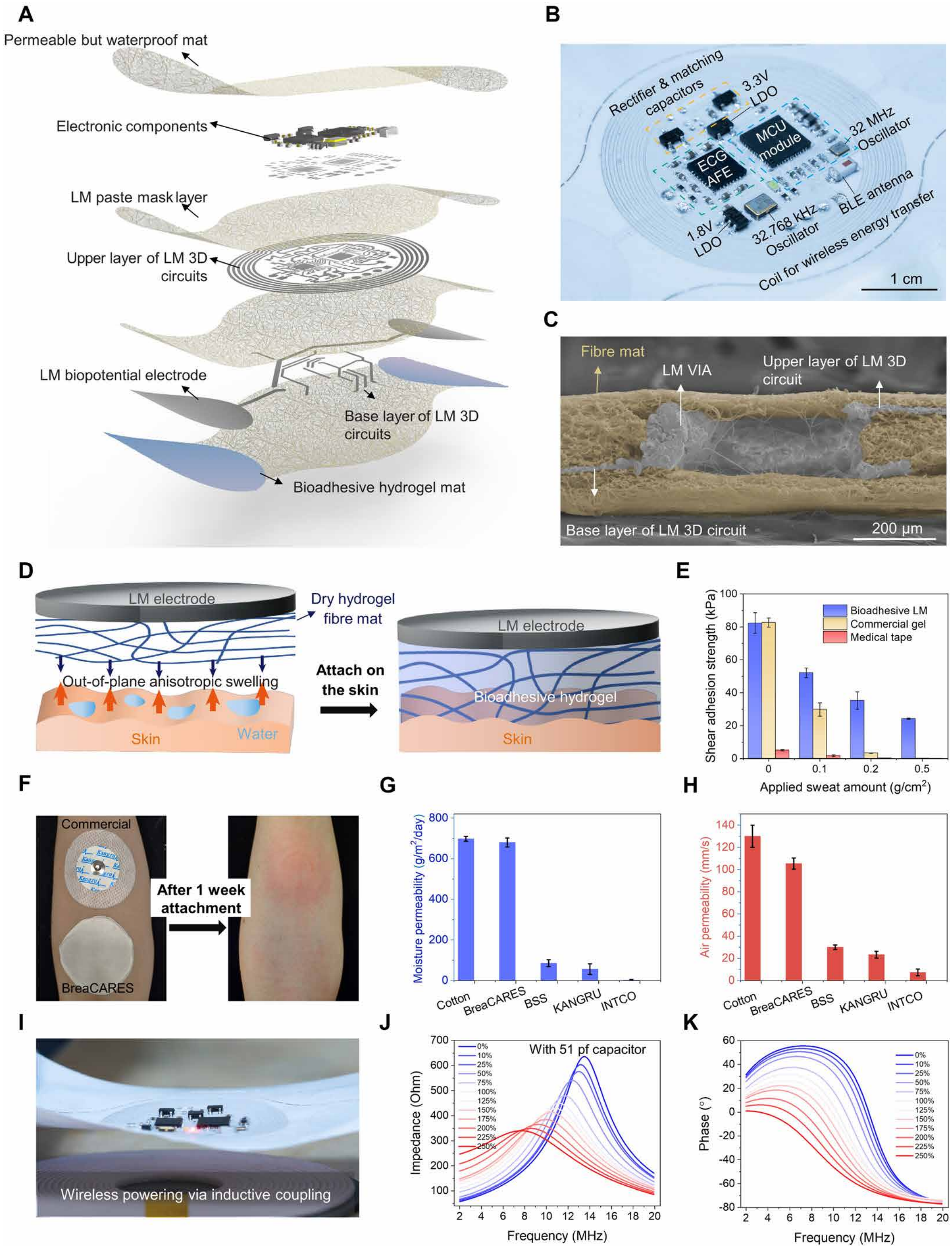

Fig. 2. Structure and properties of BreaCARES. (**A**) Exploded schematics of the BreaCARES. LM 3D microcircuits served as the reliable electrical interface between rigid components and the soft, rough, and microporous fiber mat. The bioadhesive and biofriendly user-system interface consisted of a thin electrospun hydrogel fiber mat on top of LM biopotential electrodes, enabling a stable and comfortable biointerface for long-term wear. (**B**) Digital image showing the functional modules of wireless and high-integration-density BreaCARES including ECG AFE, MCU module, LDOs, BLE antenna, oscillators, rectifier and matching capacitors, and LM coil for wireless power transfer. (**C**) Cross-sectional scanning electron microscopy image of LM VIAs for interlayer electrical connections between the upper and base layers of LM 3D circuits, while the electrical insulation was enabled by electrospun fiber mats. (**D**) Schematic illustration exhibiting the anisotropic out-of-plane swelling of dry electrospun hydrogel fiber mat upon the attachment of wet skin and the formation of bioadhesive hydrogel with robust skin adhesion. (**E**) Shear adhesion strength of bioadhesive LM, commercial gel, and medical tape with porcine skin when applying different amounts of artificial sweat. (**F**) Digital images showing the inflammatory states of skin after covering the commercial ECG electrode (brand: KANGRU) and BreaCARES electrode on the left forearm for 1 week. (**G**) Moisture permeability and (**H**) air permeability of cotton (positive control), BreaCARES electrode, and commercial ECG electrodes from brands including BSS, KANGRU, and INTCO. (**I**) Digital image of fully integrated and battery-free BreaCARES powered by wireless inductive coupling between the LM coil and the transmitter coil. (**J** and **K**) Impedance and phase of stretchable LM coil antenna at various tensile strains, respectively.

Briefly, the upper and base circuit layers (~50 μm each) including various LM micropatterns on the stretchable fibrous SBS mat were first fabricated by a combination of photolithography, pattern transfer, and stencil printing process (fig. S2). Partially oxidized LM (oLM) was subsequently stencil printed on the paste mask layer made of thin fibrous SBS (~30 μm), which was previously deposited on the upper circuit layer. The micropatterned LM 3D circuits were highly biocompatible (fig. S3), which included biopotential electrodes, stretchable antenna, interconnects, pads, and contacts (fig. S4), while the vertical electrical connections between the base and the upper layers were achieved using LM vertical interconnect accesses (VIAs; Fig. 2C).

We further formulated hybrid LM as a stretchable solder (see details in Materials and Methods), and pins of rigid electronic components, including ECG analog front end (AFE), light-emitting diodes, microcontroller unit (MCU), oscillator, Bluetooth low energy (BLE) antenna, low-dropout regulators (LDOs), and rectifier and matching capacitors, were adhered onto the printed oLM pads with additional LM pastes. The 3D integrated electrical interfaces were highly stretchable and stable, with a maximum strain of 1500% for various electronic components (figs. S5 and S6). After storing for 8 weeks, the initial electrical resistance of the LM circuit increased slightly from 0.07 to 0.11 ohms before cycling. After cycling for 8000 rounds of stretch-release (0 to 60% tensile strain), the electrical resistances only increased by 0.017 and 0.025 ohms for the freshly made sample and the stored sample at a strain of 60%, respectively (fig. S7).

We introduced a bioadhesive LM interface consisting of a thin bioadhesive hydrogel fiber mat on top of LM biopotential electrodes, enabling anisotropic out-of-plane swelling and robust adhesion upon the attachment of wet dynamic skin (Fig. 2D). The bioadhesive mat was in situ electrospun onto the LM electrode, during which the solvent (water) of the *N*-hydroxy succinimide (NHS)–grafted polyacrylic acid (PAA/NHS ester) polymer solution was adequately evaporated. When the dry bioadhesive mat contacted a wet skin surface, the bioadhesive interface absorbed interfacial water by hydration and subsequent anisotropic (only in the thickness direction) swelling, resulting in robust adhesion with the skin surface by physical cross-links and covalent cross-links of PAA/NHS ester (*44*, *45*). The bioadhesive LM electrodes displayed superior shear adhesion strength with the porcine skin under wet dynamic conditions (e.g., sweating), in comparison to medical tapes and commercial gel electrodes (Fig. 2E). The long-term on-skin attachment test was carried out by covering the left forearm skin with the commercial electrode and BreaCARES electrode for 1 week (Fig. 2F). The skin area covered by the commercial electrode displayed an inflammatory state while maintaining a relatively healthy state after the coverage of the BreaCARES electrode. The superior biocompatibility of the BreaCARES electrode resulted from the higher permeability than commercial electrodes. The moisture permeability (Fig. 2G) of the BreaCARES electrode was 7- to 347-fold higher than that of commercial ECG electrodes, and the air permeability (Fig. 2H) of the BreaCARES electrode was 2.4- to 13-fold higher than that of commercial ECG electrodes.

The BreaCARES was operated in either battery-free mode or battery-powered mode with commercial lithium-ion batteries. For battery-free BreaCARES, an embedded LM antenna can receive power wirelessly supplied by inductive coupling with the external transmitter antenna (Fig. 2F and movie S1). By tuning the inductance of the receiver coil and matching it with appropriate capacitors, the LM antenna was configured at a set resonant frequency of 13.56 MHz, which matched the frequency of the wireless power transmission signal and could attain an optimized energy efficiency. The received radio frequency ac signal was then rectified by a full-wave bridge rectifier and filtered into a dc signal by a large capacitor. The dc signal was then fed into LDOs and regulated to a stable 3.3- and 1.8-V power supply for the MCU and AFE, respectively. Finite element analysis (FEA) indicated that the stress distribution of the intrinsically stretchable LM antenna was very uniform at different tensile strains (fig. S8), which benefited high electromagnetic stability in the impedance (Fig. 2G) and phase (Fig. 2H) and the S_{11} performance of the LM coil (fig. S9) within the readable frequency. When stretched to uniaxial 30% strain, the resonance frequency decreased by 4.7% with a frequency value of 13.50 MHz. When stretched to uniaxial 60% strain, the resonance frequency decreased by 12.2% with a frequency value of 12.43 MHz.

Validation in animal models

We monitored various ECG arrhythmias in animal models using the BreaCARES coupled with a smartphone and deep learning algorithms (Fig. 3A). The ECG arrhythmias were induced by delivering the drug consisting of calcium chloride, which increased the levels of calcium in the blood, disrupted the heart's electrical impulses, and thus led to abnormal heart rhythms (*46*–*48*). Short-time Fourier transform (STFT) was used to transform the time-domain signals into a time-frequency representation (Fig. 3B). Furthermore, a data augmentation procedure was implemented to enhance the dataset of ECG signal images for cardiac event classification (see details in Materials and Methods). We adopted a convolutional neural network (CNN) to conduct the condition classification of these cardiac events with a classification accuracy of 98.387% for the prediction (Fig. 3C). From Fig. 3D, the resulting spectrograms provided a clear and distinct visualization of the different types of ECG events (fig. S10) consisting of onset of drug delivery (normal state; fig. S11), atrioventricular block (AV block; fig. S12), atrial fibrillation (AF; fig. S13), ventricular flutter (VFL; fig. S14), ventricular fibrillation (VF; fig. S15), and the final death (fig. S16). These spectrograms exhibited unique patterns in the time-frequency domain, reflecting the distinct nature of each cardiac event. Right after the surgery, distinct differences in the morphology between the control sample and the drug-induced sample were found from the hematoxylin and eosin staining results of heart slices (fig. S17).

Volunteer study of BreaCARES for personalized health care

In comparison to the commercial hard-wired and bulky ECG apparatus, BreaCARES offers several advantages such as being thin and lightweight, high signal quality and stability, wearing comfort, and biocompatibility to skin health. The whole cardiac electronic system was wireless and portable, enabling noninvasive, continuous, and real-time monitoring of cardiac health (Fig. 4A and movie S2). The bioadhesive LM electrodes had a lower skin impedance (Fig. 4B) than the commercial Ag/AgCl gels, offering higher signal-to-noise ratios and signal stability during various daily activities such as sleeping, sitting, walking, and exercising (Fig. 4, C and D). Furthermore, BreaCARES was capable of providing continuous and comfortable cardiac monitoring for 9 days (Fig. 4E). We monitored the ECG signals of 18 volunteers from different gender and age groups (<24, 24 to 40, and >40 years old) under resting states and exercising states (Fig. 4, F to M). The average heart rate values under

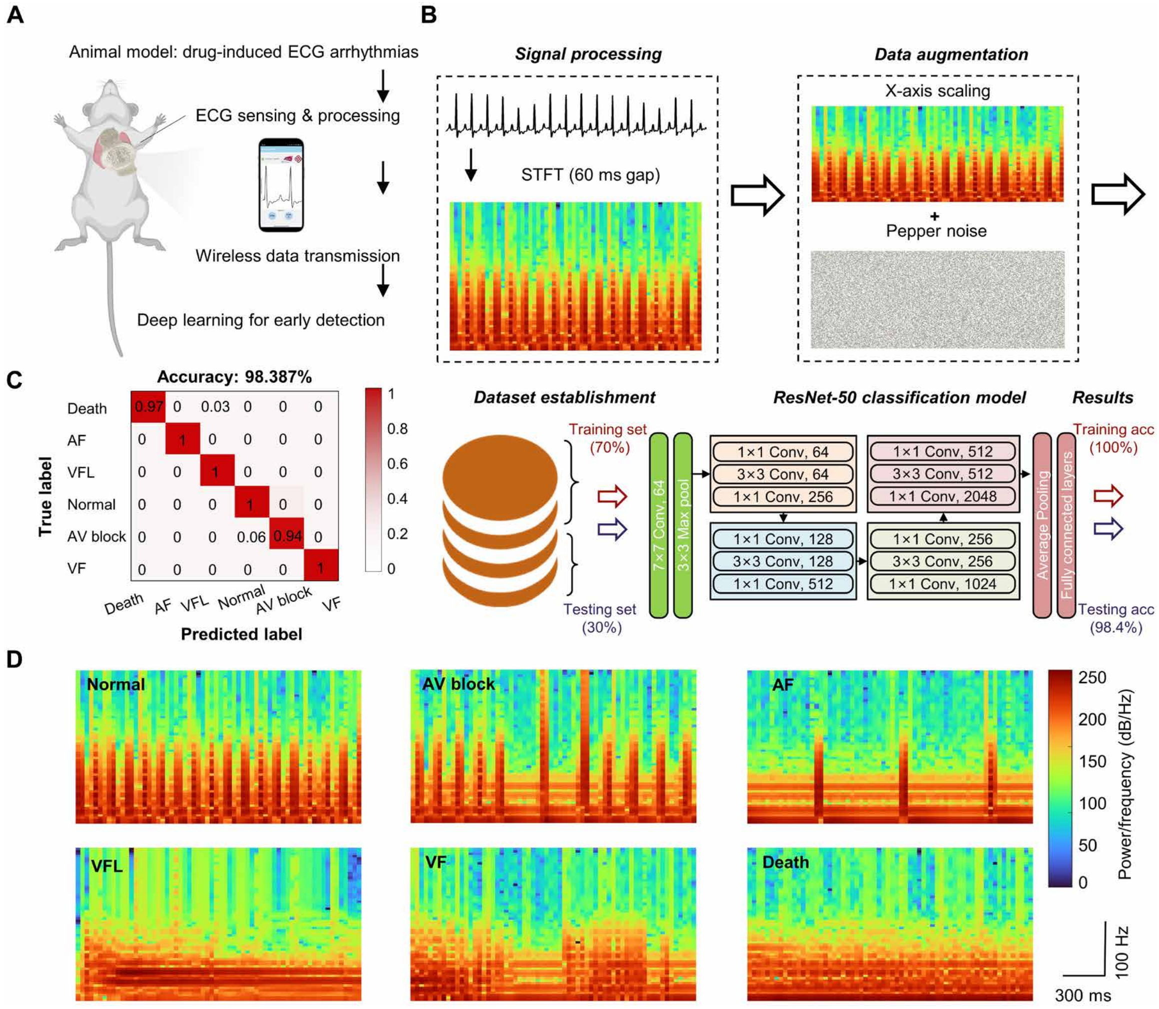

Fig. 3. Functional validation of BreaCARES in animal models. (**A**) Schematic illustration of BreaCARES integrated with deep learning algorithms for detection and classification of drug-induced ECG arrhythmias in a rat model. (**B**) Processing flow of condition classification of cardiac events obtained with BreaCARES using CNN, which included original ECG signal processing, data augmentation, dataset establishment, ResNet-50 classification, and output of results. (**C**) Accuracy classification of CNN of six cardiac events including normal state, AV block, AF, VFL, VF, and the final death. (**D**) Spectrograms of six cardiac events exhibiting unique patterns in the time-frequency domain.

the exercising state were higher than those under the resting state for both males and females. The heart rate of the middle-aged (aged 24 to 40 years old) group was higher than those of the other groups. Important intervals such as PR, QRS, and QT intervals under resting states and exercising states were also investigated among different age and gender groups.

BreaCARES in clinical translations and adoptions

To evaluate the performance of BreaCARES, we compared the diagnostic accuracy, reliability, and stability in comparison with the clinical gold standard, i.e., standard bedside ECG monitors in the cardiovascular ICU. Several ICU clinically proven ECG monitors were adopted including GE MAC 800 Resting ECG System (MAC 800, GE Healthcare), Mindray vital sign monitor (BeneView T8, Mindray USA), and GE Solar 8000 M Patient Monitor (Solar 8000M, GE Healthcare). To achieve long-distance (meter-scale) and continuous monitoring, we adopted the battery-powered BreaCARES for clinical translations, including outpatient early diagnosis of heart diseases, stable intraoperative monitoring, and ICU-grade continuous 24-hour postoperative monitoring. In comparison to the clinical gold standard, i.e., standard vital sign monitors in the operating room or in the ICU, BreaCARES exhibited comparable accuracy with the standard monitors while maintaining superior stability.

First, BreaCARES served as a portable outpatient preoperative detection tool with hospital-grade accuracy while exhibiting interference-free stability (fig. S18 and movie S3) and superior wearing comfort (Fig. 5A). Seven typical heart diseases including sinus bradycardia (SB), MI (movie S4), ST-elevation MI (STEMI; fig. S19), STEMI with tachycardia (Tachy), AF, atrial flutter (AFL; Fig. 5B and movie S5), and ventricular premature beats (VPB; fig. S20 and movie S6) were clearly diagnosed by the BreaCARES (Fig. 5C). The signals from BreaCARES displayed similar waveforms and features to those from the hospital machine. The diagnostic result assisted by the long short-term memory (LSTM) neural network was 98.7% accurate with those from clinical diagnosis (Fig. 5D). Notably, after removing the BreaCARES, no adverse effects were caused on the skin. However, erythema and

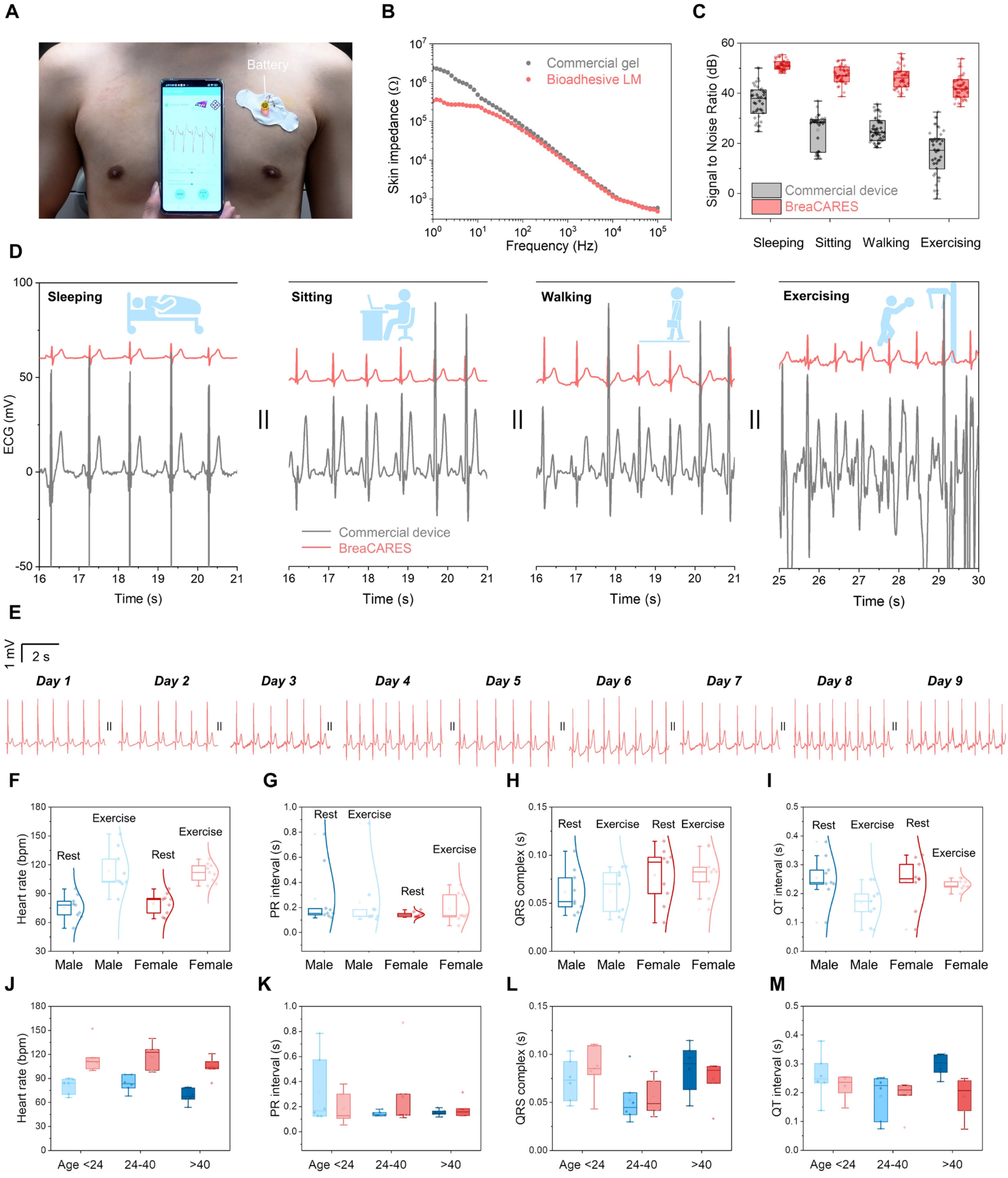

Fig. 4. Continuous ECG data collection and analysis for personalized health care. (**A**) Digital image of wireless BreaCARES for continuous on-skin ECG monitoring. (**B**) Skin impedance of the commercial gel electrode and bioadhesive LM electrode as the function of frequency. (**C** and **D**) Statistical results of signal-to-noise ratios and ECG signals of a commercial ECG device and BreaCARES under various daily activities (sleeping, sitting, walking, and exercising), respectively. (**E**) Continuous and wireless ECG monitoring of an adult volunteer (male, aged 27) for 9 days. (**F** to **I**) Statistical results of heart rates, PR intervals, QRS complex, and QT intervals from ECG signals of 18 volunteers at resting states and exercising states as the functions of gender. (**J** to **M**) Statistical results of heart rates, PR intervals, QRS complex, and QT intervals from ECG signals of 18 volunteers at resting states (blue columns) and exercising states (red columns) as the functions of age.

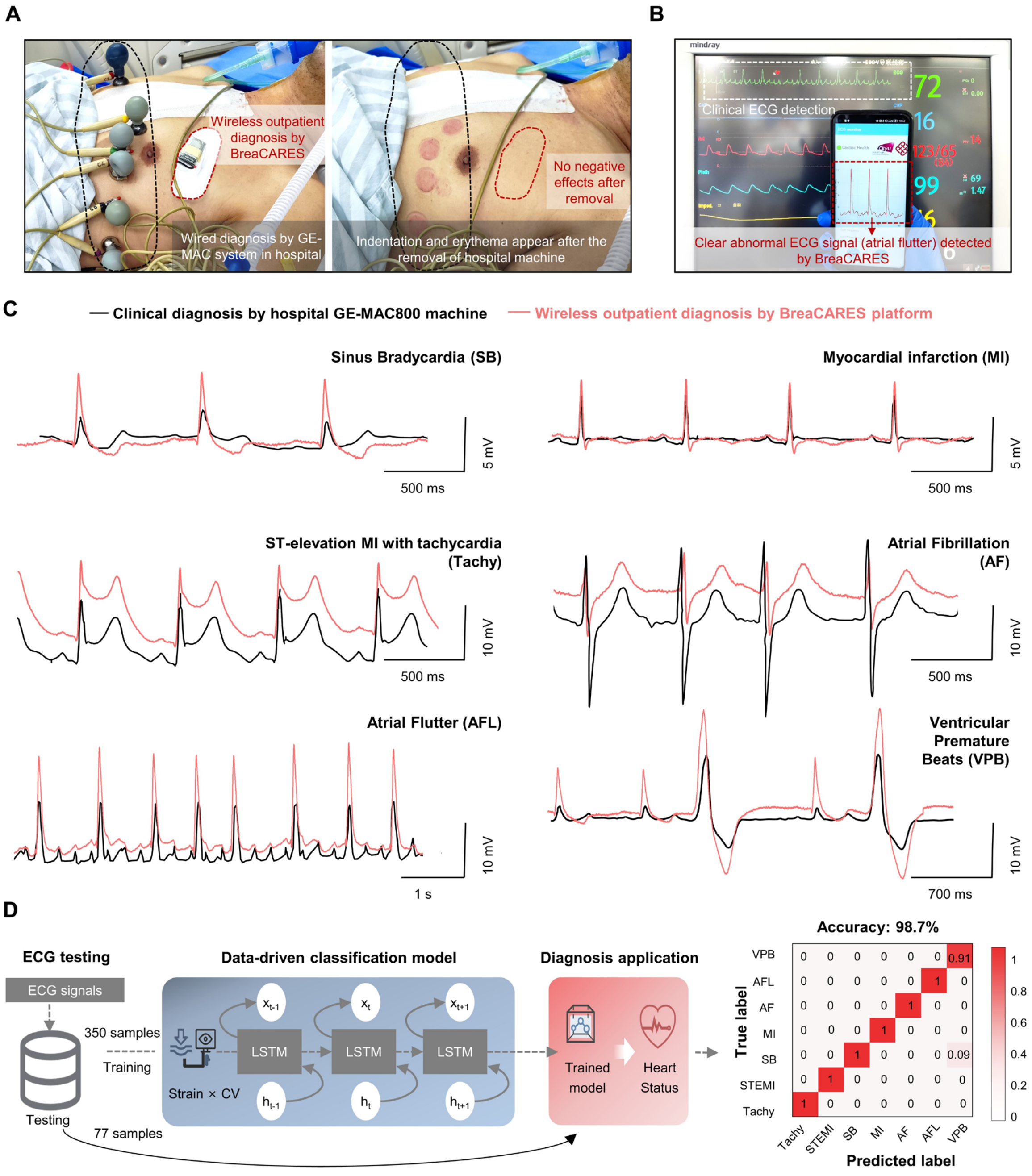

Fig. 5. BreaCARES for wireless hospital-grade outpatient early diagnosis in a cardiovascular ICU. (**A**) Digital images showing the use of wireless BreaCARES and hospital GE-MAC800 machine for the early detection of heart diseases. After removing the BreaCARES and GE-MAC800 machine, no negative effects by BreaCARES were observed, while the GE-MAC800 machine showed obvious indentation and erythema on the patient's skin. (**B**) Detection of abnormal ECG signals of AFL by a hospital ECG monitor (Mindray) and BreaCARES. (**C**) Six typical heart diseases detected by wireless BreaCARES and hospital GE-MAC800 machine including SB, MI, STEMI with Tachy, AF, AFL, and VPB. (**D**) Deep learning algorithm structure and the confusion matrix, showing the accuracy of BreaCARES for the diagnosis of various heart diseases when compared with the standard hospital monitor. The slight difference was mostly induced by the difference in the lead position between BreaCARES and the hospital monitor when collecting their ECG data at the same time because the overlapping of their lead positions cannot obtain their ECG signals simultaneously.

indentation were observed after the use of a hard-wired hospital ECG diagnostic tool (fig. S21). Therefore, when involving continuous and portable cardiac monitoring for early detection of possible cardiac diseases, the BreaCARES can serve as a hospital-grade outpatient monitor while offering a higher degree of stability, wearing comfort, and biocompatibility.

Apart from the diagnostic consistency with ICU standard monitors, reliability and stability are also of great significance for evaluating "ICU-grade accuracy." The BreaCARES was adopted for intraoperative monitoring of cardiac status during the mitral valve replacement (MVR) operation (Fig. 6, A and B), which is a surgery to replace a poorly working mitral valve with an artificial valve. First,

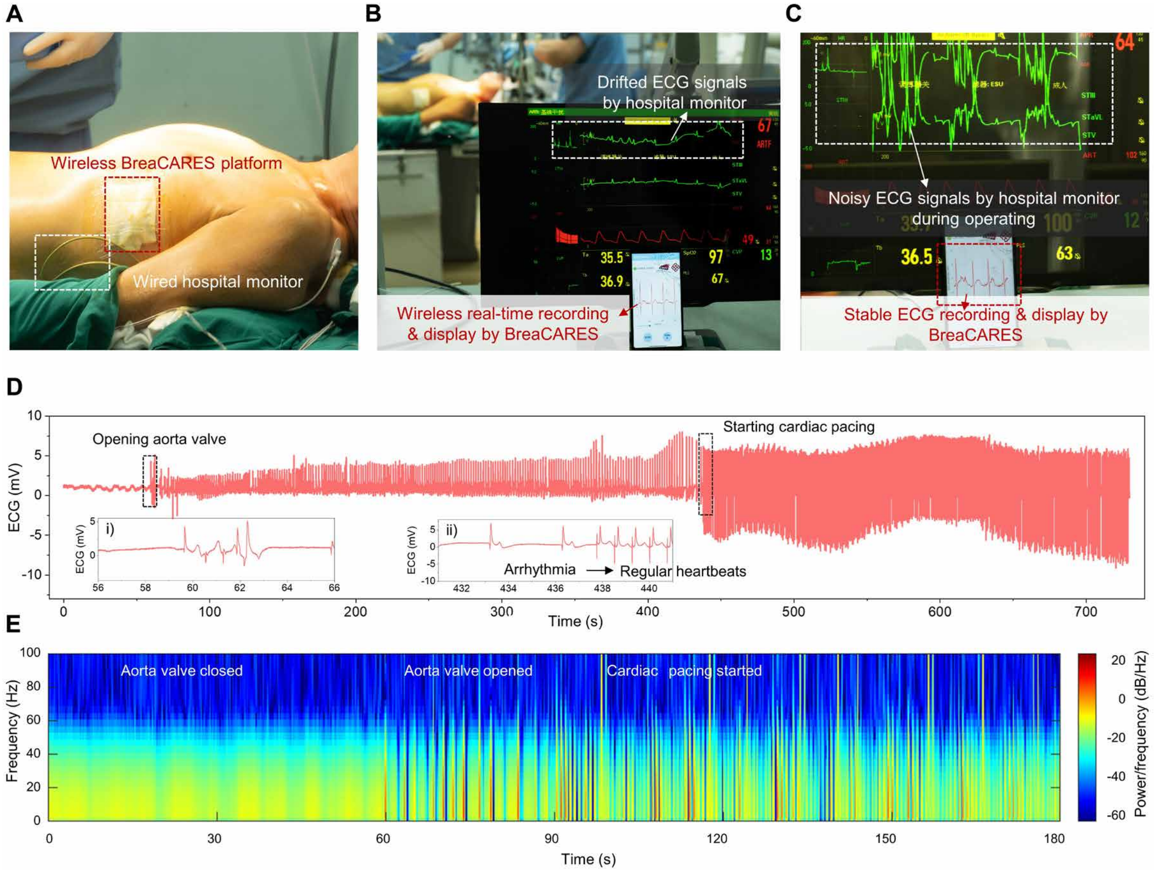

Fig. 6. BreaCARES for real-time and stable intraoperative monitoring. (**A** and **B**) Digital images showing the intraoperative monitoring of a patient during the MVR surgery using the wireless BreaCARES and clinical wired ECG monitor. (**C**) Comparison of recorded ECG signals using BreaCARES and hospital ECG monitor during the heart surgery. (**D**) Continuous and stable intraoperative ECG monitoring by BreaCARES during MVR surgery including the onset of closing the aorta valve, operating, opening of the aorta valve, and subsequent cardiac pacing for the recovery of regular heartbeats. (**E**) Spectrogram of the intraoperative ECG signals at various cardiac events including the closure and opening of the aorta valve and cardiac pacing.

the battery-powered BreaCARES successfully communicated with a smartphone and transmitted ECG data in a wireless and real-time manner (movie S7). The ECG signal recorded by the wireless BreaCARES remained very stable either in preoperative preparation (fig. S22) or during operation (Fig. 6C and movie S8), while wired hospital devices displayed drifted and noisy signals. Various cardiac states during the surgery were recorded by BreaCARES in real time, including the onset of closing the aorta valve, operating, opening of the aorta valve, and subsequent cardiac pacing for the recovery of regular heartbeats.

Specifically, after performing a median sternotomy, cardiopulmonary bypass was initiated when the heart was not actively beating, and the functions were taken over by a heart-lung machine. Throughout the surgical procedure including cardiopulmonary bypass, cardioplegia, exposure of the mitral valve, removal of the diseased valve, preparation of the mitral annulus, implantation of the new valve, and the closure of the left atrium, the recorded ECG signals had low amplitude and were irregular, corresponding to cardiopulmonary bypass or background electrical activity [image (i) in Fig. 6D]. Next, the heart was restarted, and the blood flow was gradually restored when opening the aortic valve, which resulted in sudden spikes and the emergence of irregular ECG signals. Irregular QRS complexes with varying intervals and amplitudes indicated the ECG arrhythmia after MVR surgery [image (ii) in Fig. 6D]. To resolve the ECG arrhythmia, cardiac pacing was carried out with the appearance of clear pacing spikes followed by regular, synchronized QRS complexes of ECG signals. The corresponding spectrograms of cardiac events are shown in Fig. 6E, including operating with the closure of the aorta valve, opening of the aorta valve, and subsequent cardiac pacing for the recovery of regular heartbeats.

For the postoperative cardiac care in Fig. 7, we have compared the performance of BreaCARES and the clinical gold standard for long-term monitoring, i.e., ICU vital sign monitor (GE Solar 8000M Patient Monitor, GE Healthcare). BreaCARES was further capable of providing ICU-grade postoperative monitoring continuously and comfortably (Fig. 7A and movie S9). In comparison to the wired clinical ECG monitor, the BreaCARES avoided the use of cumbersome readout devices (Fig. 7B) with superior signal quality and stability (Fig. 7C).

BreaCARES exhibited diagnostic consistency with standard ICU monitors in terms of a sequence of pathological states of the ICU patient during the long-term monitoring (Fig. 7, D and E). At the first hour of monitoring, postoperative T-wave inversion ECG signals were recorded, potentially indicative of myocardial ischemia after the heart

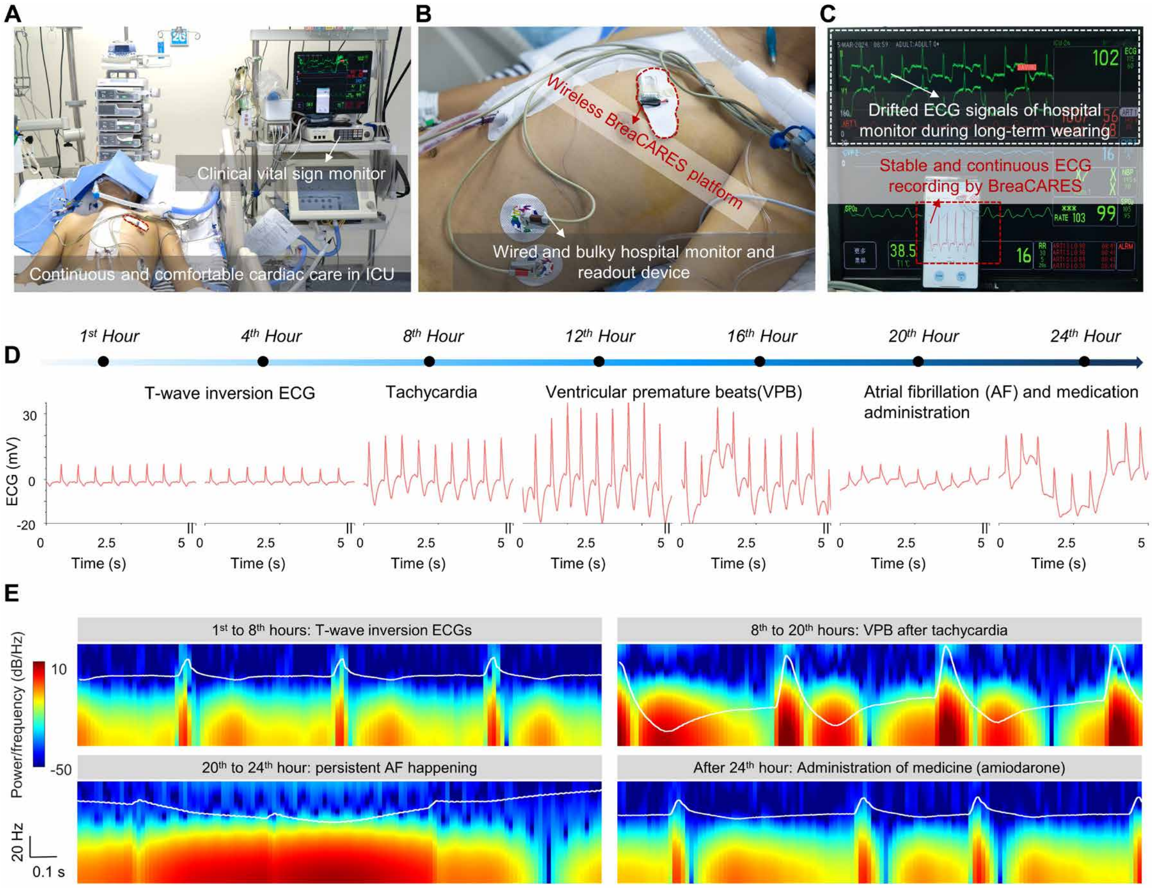

Fig. 7. BreaCARES for ICU-grade inpatient continuous postoperative monitoring for 24 hours. (**A** and **B**) Digital images showing the intraoperative ECG monitoring of a patient using wireless BreaCARES and clinical wired and bulky ECG monitor. (**C**) Comparison of postoperative ECG signals using wireless BreaCARES and clinical wired ECG monitor. (**D**) Continuous and real-time postoperative inpatient monitoring by wireless BreaCARES in cardiovascular ICU for 24 hours, during which various cardiac arrhythmias of the patient were clearly detected including ECG T-wave inversion, Tachy, VPB after Tachy, persistent AF happening, and post-AF ECG signals from the medication administration of amiodarone. (**E**) Spectrograms of a variety of postoperative ECG signals including T-wave inversion ECGs, VPB after Tachy, persistent AF happening, and post-AF ECG signals from the medication administration of amiodarone.

surgery. After 8 hours, high-frequency waveforms with a marked increase in amplitude by ~3.2-fold were recorded, suggesting a supraventricular Tachy. The Tachy ECG abnormalities lasted for more than 4 hours, with the appearance of irregular oscillations with significant amplitude fluctuations in the VPB ECG signals, which mainly resulted from abnormal electrical activity in the ventricles after the heart surgery. After continuous monitoring for more than 20 hours, we observed the occurrence of persistent AF, of which many f waves appeared with the weakened/missing P waves, QRS complexes, and T waves in the ECG signals. The f waves had high frequency and low amplitude, which were more clearly identified in the spectrograms in Fig. 7E. After 24 hours, the medication administration of amiodarone resulted in the partially missing f waves, indicating the gradual recovery from the AF arrhythmia (Fig. 7F).

DISCUSSION

Existing clinical equipment in established inpatient settings is usually multiple hard wired, specialist required, invasive, and cumbersome. In contrast, digital health technologies based on soft and wearable electronic devices and systems potentially enable noninvasive, on-body, and portable health care monitoring and improve personalized patient outcomes.

Nevertheless, existing wearable technologies still suffer from unaddressed gaps in clinical translations and adoptions owing to difficulties in achieving medical-grade accuracy with real-time and sufficient datasets for clinical decision-making and poor patient/consumer compliance from impermeable and bulky form design factors and integrations.

Our proposed BreaCARES is the ICU-grade and breathable type of cardiovascular digital health platform for health care, outpatient diagnostics, and intraoperative and postoperative monitoring, exhibiting ICU-grade accuracy while having superior anti-interference stability, portability, and long-term on-skin biocompatibility to the clinically and commercially available cardiac monitors in ICUs. In comparison to conventional bulky and hard-wired single-lead or multilead monitors, inherent advantages of BreaCARES such as medical-grade accuracy, superior portability, compactness (miniaturization and lightweight), biocompatibility, and wearing comfort have been demonstrated. Nevertheless, the single-lead design also limits the diagnostic capability for complex conditions as it only provides a single view of the heart's electrical activity on each lead placement. In conclusion, BreaCARES can serve as a superior wireless single-lead ECG monitor and a complement tool for multilead monitors in various clinical studies including outpatient diagnostics, intraoperative monitoring, and postoperative inpatient cardiac care in ICUs.

To our knowledge, BreaCARES is one of the most advanced cardiac systems in terms of permeability, integration complexity, sampling frequency, continuity, biocompatibility, and comprehensive clinical practices (table S1). We envision that BreaCARES will become a novel cardiac care platform with both medical-grade accuracy and wearing comfort over long term and large populations, which is compatible with both established inpatient and outpatient health care settings.

MATERIALS AND METHODS

Materials

Solvents were purchased from Anaqua Global International Inc., Ltd. The photoresist (NR9-1500P) and the developer for NR9-1500P (DR6) were purchased from Futurrex, Inc., US. LM was obtained from Sigma-Aldrich. All materials were used as received.

Fabrication of BreaCARES

The fabrication of permeable stretchable 3D integrated LM circuit board (LM antennas, traces, connections, contacts, electrodes, VIAs, various electronic components, etc.) followed previously developed protocols (*43*), in which the stretchable and stable 3D electrical interfaces were achieved by LM hybrid solders. The biocompatible and bioadhesive mat was deposited onto the LM biopotential electrodes by direct electrospinning of PAA/NHS ester polymer solution {10 wt % PAA, 0.4 wt % *N*-hydroxysuccinimide, 0.8 wt % 3-[(ethylimino) methylidene]amino-*N*,*N*-dimethylpropan-1-amine, and water as the solvent}. The BreaCARES typically adopted BLE-integrated MCU (CC2640, Texas Instruments) to achieve data acquisition, transmission, and functional control. Code Composer Studio was used for MCU programming. A 3.3-V LDO (TPS76933, Texas Instruments) was used to provide a stable power supply for the MCU. A biopotential sensing chip (MAX30003, Analog Devices) was used as the AFE for ECG sampling (sampling rate: 500 Hz). A 1.8-V LDO and a 32.768-kHz crystal were equipped for driving the sampling of the AFE. The data were read by the MCU through serial peripheral interface communication and then were transmitted to the mobile device wirelessly through BLE 5.0 and plotted in real time on the graphical user interface of the Android application (developed by Android Studio 2022.2.1). An inductive coil and capacitors that set the resonant frequency at 13.56 MHz enabled wireless power supply or charging. The received radio frequency signals were rectified with a full wave bridge rectifier with a smoothing capacitor. A hybrid LM solder was formulated by using oLM (80°C, 16 hours) as the contact pads and pristine LM as the paste connecting LM circuits and the pins of electronic components. Pins of rigid electronic components, including ECG AFE, light-emitting diodes, MCU module, oscillator, BLE antenna, LDOs, and rectifier and matching capacitors, were adhered onto the printed oLM pads with additional LM pastes. Last, the whole monolithic BreaCARES microelectronic system was encapsulated with another electrospun SBS fiber mat. Here, the "permeable but waterproof mat" was obtained by electrospinning the SBS fiber mat directly onto the existing electronic system. The SBS polymer solution was prepared by dissolving the SBS polymer in the mixed solvent including tetrahydrofuran and dimethylformamide (volume ratio, 3:1) with a weight ratio of 13 wt %. The set voltage was 18 kV, and the collecting distance was 15 cm. For the battery-powered BreaCARES design, we have two types of batteries for short-term and long-term cardiac monitoring. The former was a small coin cell–sized battery (LIR1040; diameter, 10 mm; height, 4 mm) with a capacity of 35 mAh. The latter was a large-sized battery (DDH 702030; length, 30 mm; width, 20 mm; height, 7 mm) with a capacity of 300 mAh. Specifically, when in standby mode (Bluetooth was not connected, and the sampling process started), the current consumption of the circuit was less than 2 mA; at sampling mode (Bluetooth was connected, the sampling process started, and data streaming started), the current was less than 3 mA. Thus, the short-term-use battery could support the circuit continuously running for at least 11.7 hours, and the long-term-use battery could support for at least 100 hours.

Characterizations

The morphology of LM 3D circuits including fiber mats, upper and base layers of LM traces, and LM VIAs was observed by scanning electron microscopy (TESCAN VEGA3). The electrical resistance of resistors and capacitors connected with hybrid LM solders under different strains was measured by a four-terminal method with a source meter (Keithley 2400) coupled with a customized stretching deep (Zolix). The impedance and phase of the LM coil antenna were explored by an impedance analyzer (E4991B, Keysight Technologies). Moisture permeability tests were performed under the standard E96/E96M-13 by the cup method (temperature, 22°C; humidity, 63%; 72 hours). The shear adhesion strength was tested according to Standard ASTM 2255. Porcine skin was purchased from the local market. Porcine skin, bioadhesive LM, medical tape (3 M), and commercial gel (3 M) were cut into pieces (2.5 cm by 5 cm). The overlapped area of porcine skin and each group was set as 2.5 cm^2. Free ends of the adhered samples were clamped onto the universal testing machine (Instron 5566) with a load cell of 500 N and a testing speed of 50 mm/min. The average peak force was recorded and divided by the adhered area (i.e., 2.5 cm^2) to obtain shear adhesion strength. Different amounts of artificial sweat (pH, 4.7 ± 0.1; Zhongwei Equipment) were applied onto the porcine skin to test the wet adhesion strength, mimicking the sweating process. The skin impedance of LM biopotential electrodes and commercial gel electrodes was tested by an electrochemical workstation (CHI 660) using the electrochemical impedance spectroscopy technique. The distance between testing electrodes adhered to the skin surface was set as 5 cm. Impedance and phase angle as the function of frequency ranging from 1 to 10,000 Hz were recorded by an ac sinusoid signal amplitude of 10 mV. The samples for moisture and air permeability tests included BreaCARES electrodes, a positive control sample (cotton fabric), commercial ECG electrodes, and samples from three brands including KANGRU, BSS, and INTCO. The moisture permeability of BreaCARES electrodes and commercial electrodes was tested on the basis of the E96/E96M-13 standard (cup method) with a testing duration of 72 hours. The air permeability of various electrodes was tested according to the ASTM D737-08 standard with a MO21S air permeability tester (SDL America) at the airflow pressure of 100 Pa. The S_{11} data were measured by an Agilent 8753ES S-parameter network analyzer in the frequency range between 8 and 20 MHz, with an electro-magnetic interference near-field probe (transmitting coil; diameter, ~6 cm). The resonance frequency changed from 14.16 MHz (0%) to 12.43 MHz when 60% uniaxial stretching strain was applied.

Finite element analysis (FEA)

Static structural mechanics of the stretchable LM coil antenna were analyzed by FEA. Material mechanical parameters and output results are summarized in table S2. The LM coil antenna was subjected to a series of biaxial mechanical tensions ranging from 0 to 200% tensile strains. The stress responses were collected. The ratio of the maximum stress to the average stress was adopted as the stress concentration factor, i.e., $\sigma_{max}/\sigma_{avg}$.

Cell cytotoxicity test

C2C12 cells (Servicebio) were used to examine the in vitro cytotoxicity of materials for cardiac electronic skin including SBS mat, PAA/NHS ester mat, and LM circuit. Briefly, 5×10^3 C2C12 cells in 200 μl of full Dulbecco's modified Eagle's medium (Servicebio) supplemented with 10% fetal bovine serum (Servicebio) and 1% penicillin/streptomycin (Servicebio) were seeded in a 96-well plate. The fresh full medium and 20% dimethyl sulfoxide/full medium mixture were used as the blank and negative control, respectively. All samples were cultured at 37°C in an incubator with 5% CO_2. After 24 hours of incubation, CCK-8 assays were used to quantify the cell viability. The cell viability was determined using the absorbance ratio between the tested well and the blank control well. In addition, calcein-AM/propidium iodide (calcein-AM/PI) staining was used to test the cell proliferation and viability. Similarly, C2C12 cells were seeded in a 24-well plate. After a 24-hour incubation, the medium from the culture plate was discarded and 1 ml of fresh full medium was added. Then, 0.2-cm^2 sterile samples were directly added to the 24-well plate to evaluate the cytotoxicity of the materials. The fresh full medium and 20% dimethyl sulfoxide/full medium mixture were used as the blank and negative control, respectively. After incubation for 1, 2, and 3 days, calcein-AM/PI staining was used to observe live and dead cells in different groups according to the manufacturer's protocol. Briefly, after discarding the culture medium, a 200-μl phosphate-buffered saline staining solution with 0.4 μl of Calcein-AM and 0.4 μl of PI was added and incubated for 30 min. After rinsing with phosphate-buffered saline, cells were observed using a fluorescence microscope (Nikon Ti2-E).

Animal experiment, cryosection, histological staining, and observation of heart slices

All animal experimental procedures were approved by the Institutional Animal Care and Use Committees at the City University of Hong Kong (AN-STA-00000274). Male Sprague-Dawley rats (aged 10 weeks, ~300 g, $n = 3$) were first treated with gaseous anesthesia (isoflurane, 3%). Surface ECG signals were recorded using the BreaCARES wirelessly connected to a smartphone. After rapid intravenous injection of calcium chloride ($CaCl_2$, Aladdin Bio-chem Technology Co.) solution at a dose of 0.4 mg/kg (dissolved in saline at a concentration of 0.1 g/ml), abnormal ECG signals were recorded simultaneously. Last, the rats were euthanized using carbon dioxide. The rats in the control group received an equivalent volume of normal saline and were subsequently euthanized with carbon dioxide. Next, the heart tissues of rats were collected for histological evaluation. Briefly, heart tissues were fixed in 4% paraformaldehyde and then dehydrated in a sucrose gradient solution (i.e., 10, 20, and 30%). After being embedded in an optimal cutting temperature compound, these tissues were frozen sectioned using a freezing microtome (Cryostar NX70, Thermo Fisher Scientific) with a section thickness of 14 μm. Subsequently, the slice samples were stained with a hematoxylin-eosin staining kit (Solarbio), sealed using neutral balsam (Biosharp, Life Sciences), and observed and photographed using a light microscope (Nikon).

STFT procedure of ECG signals

In this study, a comprehensive batch of ECG signals was collected, representing a range of cardiac events including the normal state, AV block, AF, VFL, VF, and the final death. Here, the specific size of the dataset was 102 each × 6 types = 612 in total. A sampling frequency of 500 Hz was selected, which was adequate for capturing the essential details in ECG signals, as it was well above the Nyquist rate for the highest-frequency components typically present in such signals. The diversity in these signals encapsulated the complexity of cardiac rhythms and their respective pathophysiological states. ECG signals from six cardiac events during the drug delivery process were clearly recorded by wireless BreaCARES (fig. S10). Original ECG signals were not directly applicable to the input form of CNNs; therefore, STFT was used to transform the time-domain signals into a time-frequency representation. The continuous STFT was

$$X(t,f) = \int_{-\infty}^{\infty} \omega(t-\tau)x(\tau)e^{-j2\pi f\tau}d\tau \tag{1}$$

where $\omega(t-\tau)$ is the window function, f is the frequency parameter, $x(\tau)$ is the original signal, and X is the transformed signal. Because the collected signal is always discrete, we used the discrete STFT here

$$X(n,f) = \sum_{m=-\infty}^{\infty} \omega(n-m)x(m)e^{-j2\pi fm} \tag{2}$$

This transformation allowed us to observe not only the presence of various frequency components but also how these components varied over time, which was a crucial aspect when dealing with nonstationary signals such as ECG. During STFT, a window length of 36 was used to balance the resolution in the time-frequency domain, with an overlap of 20 to ensure continuity and preserve information between adjacent frames. The window function was set as the Hamming window

$$\omega(n) = a_0 - (1-a_0)\cos\left(\frac{2\pi n}{N-1}\right) \tag{3}$$

where $a_0 = 0.53836$. The number of fast Fourier transform points was set to 36, which guarantees the proper frequency resolution. A gap of 30 was maintained between successive STFT computations to reduce computational load without sacrificing the temporal resolution. Last, the STFT output images were resized to 224 by 224 pixels, a dimension suitable for feeding into neural network models without significant loss of information.

Data augmentation

Biological procedures were hard to control, so the sample number varies among different classes, and some of them may be insufficient to form qualified neural network input. To address these scenarios, we used data augmentation techniques. The following description outlined the data augmentation procedure implemented to enhance the dataset of ECG signal images for cardiac event classification. To ensure an adequate number of examples in each category, a target number of 102 images per category were set. The augmentation process was applied to any category that did not meet this threshold. The augmentation was performed using MATLAB and defined by two primary transformations. First, additional salt-and-pepper noises were added by a 15% noise density. Second, to simulate slight variations in the ECG signal from different heart rates, these images were further scaled along the x axis between 90 and 110% randomly of their original size. By using these data augmentation methods, the dataset gained variety and volume, which improved the generalization ability of a deep learning model trained on it. The augmented dataset better represented the variability encountered in real-world scenarios, thus enhancing the robustness of the subsequent classification task.

Cardiac condition recognition by a deep network

We used a CNN model to conduct the condition classification. Once the data store was initialized, the dataset was automatically split into two parts: 70% of the data were used for training the model, while the remaining 30% were reserved for validation. The split was randomized to ensure that both sets were representative of the overall dataset. The network was trained using the stochastic gradient descent with momentum optimizer. Training options were configured with an initial learning rate of 0.01, a maximum of 10 epochs, and a minibatch size of 64. A shuffle operation for the training data before each epoch was deployed to prevent the network from learning the order of the training data, which improved generalization. The training procedure was conducted on a RTX 2080 GPU platform with 16G RAM and i7 Intel CPU.

Volunteer and clinical practices

All procedures in the on-skin attachment of BreaCARES on the volunteers followed ethical guidelines (HSEARS20230101001), which were approved by The Hong Kong Polytechnic University. The long-term on-skin attachment test was carried out by covering the left forearm skin with the commercial electrode (KANGRU) and BreaCARES electrode for 1 week. The clinical practices of BreaCARES followed ethical guidelines (KY-H-2024-020-08) in Guangdong Provincial People's Hospital of Southern Medical University. Hospital ECG monitors including the GE-MAC800 system, GE Solar 8000M Patient Monitor, and Mindray vital sign monitor were adopted. The ECG lead was mainly placed at the left sternal border, specifically at the fourth intercostal space, as it provides information about the anterior and lateral walls of the heart. For intraoperative ECG monitoring during MVR surgery, the surgeons put the recording electrodes separately while keeping them away from the surgical field, i.e., the left side of the chest. In this way, the operating noise and pressure have been largely mitigated on either the clinical electrode (near shoulder) or BreaCARES electrode (side). The positional difference is inevitable when comparing the performance of BreaCARES with the standard monitor because it was impractical to overlap their recorded skin area while collecting their ECG data at the same time.

Seven types of ECGs were collected from different patients, including MI, STEMI, STEMI with Tachy, SB, AF, AFL, and VPB. The signals were segmented into 427 samples for training and testing, with the labels determined by experienced cardiac surgeons. These samples were divided into a training set of 350 samples and a testing set of 77 samples. To improve the processing efficiency when managing long-term dependencies, we further adopted LSTM—a type of recurrent neural network architecture designed to model sequential data and capture long-range dependencies. ECG data collected from gold standard ICU ECG monitors and BreaCARES were directly input into LSTM. The confusion matrix revealed a single misclassification in the SB category, potentially due to baseline drift. The model was trained on a deep learning workstation equipped with an Intel i7 14700 CPU, Nvidia RTX 4060Ti GPU, and 32GB RAM. The LSTM network used a tanh activation function for state transitions and a sigmoid function for gate operations, with a cross-entropy loss function to optimize performance.

Supplementary Materials

The PDF file includes:

Figs. S1 to S22
Tables S1 and S2
Legends for movies S1 to S9
References

Other Supplementary Material for this manuscript includes the following:

Movies S1 to S9

REFERENCES AND NOTES

1. GBD 2021 Forecasting Collaborators, Burden of disease scenarios for 204 countries and territories, 2022–2050: A forecasting analysis for the Global Burden of Disease Study 2021. *Lancet* **403**, 2204–2256 (2024).
2. H. Hu, H. Huang, M. Li, X. Gao, L. Yin, R. Qi, R. S. Wu, X. Chen, Y. Ma, K. Shi, C. Li, T. M. Maus, B. Huang, C. Lu, M. Lin, S. Zhou, Z. Lou, Y. Gu, Y. Chen, Y. Lei, X. Wang, R. Wang, W. Yue, X. Yang, Y. Bian, J. Mu, G. Park, S. Xiang, S. Cai, P. W. Corey, J. Wang, S. Xu, A wearable cardiac ultrasound imager. *Nature*, *613* , 667–675 (2023).
3. C. Wang, X. Chen, L. Wang, M. Makihata, H.-C. Liu, T. Zhou, X. Zhao, Bioadhesive ultrasound for long-term continuous imaging of diverse organs. *Science* **377**, 517–523 (2022).
4. J. A. Rogers, A transient, closed-loop network of wireless, body-integrated devices for autonomous electrotherapy. *Science* **376**, 1006–1012 (2022).
5. S. A. Williams, P. Ganz, Response to comment on "A proteomic surrogate for cardiovascular outcomes that is sensitive to multiple mechanisms of change in risk". *Sci. Transl. Med.* **14**, eadd1355 (2022).
6. R. Yagi, Y. Mori, S. Goto, T. Iwami, K. Inoue, Routine electrocardiogram screening and cardiovascular disease events in adults. *JAMA Intern. Med.* **184**, 1035–1044 (2024).
7. M. J. M. Cluitmans, L. R. Bear, U. C. Nguyên, B. van Rees, J. Stoks, R. M. A. Ter Bekke, C. Mihl, J. Heijman, K. D. Lau, E. Vigmond, J. Bayer, C. N. W. Belterman, E. Abell, L. Labrousse, J. Rogier, O. Bernus, M. Haïssaguerre, R. J. Hassink, R. Dubois, R. Coronel, P. G. A. Volders, Noninvasive detection of spatiotemporal activation-repolarization interactions that prime idiopathic ventricular fibrillation. *Sci. Transl. Med.* **13**, eabi9317 (2021).
8. K. Shivkumar, S. M. Narayan, Imaging cardiac arrhythmias. *Sci. Transl. Med.* **3**, 98fs2 (2011).
9. F. Khan, "ECG in the ICU patient: Identification and treatment of arrhythmias in the intensive care unit," in *Electrocardiogram in Clinical Medicine* (John Wiley & Sons Ltd., 2020), pp. 345–357.
10. D. Jung, C. Lim, H. J. Shim, Y. Kim, C. Park, J. Jung, S. I. Han, S. H. Sunwoo, K. W. Cho, G. D. Cha, D. C. Kim, J. H. Koo, J. H. Kim, T. Hyeon, D. H. Kim, Highly conductive and elastic nanomembrane for skin electronics. *Science* **373**, 1022–1026 (2021).
11. Y. Shin, H. S. Lee, Y. J. Hong, S.-H. Sunwoo, O. K. Park, S. H. Choi, D.-H. Kim, S. Lee, Low-impedance tissue-device interface using homogeneously conductive hydrogels chemically bonded to stretchable bioelectronics. *Sci. Adv.* **10**, eadi7724 (2024).
12. Z. Jiang, N. Chen, Z. Yi, J. Zhong, F. Zhang, S. Ji, R. Liao, Y. Wang, H. Li, Z. Liu, Y. Wang, T. Yokota, X. Liu, K. Fukuda, X. Chen, T. Someya, A 1.3-micrometre-thick elastic conductor for seamless on-skin and implantable sensors. *Nat. Electron.* **5**, 784–793 (2022).
13. J. Yi, G. Zou, J. Huang, X. Ren, Q. Tian, Q. Yu, P. Wang, Y. Yuan, W. Tang, C. Wang, L. Liang, Z. Cao, Y. Li, M. Yu, Y. Jiang, F. Zhang, X. Yang, W. Li, X. Wang, Y. Luo, X. J. Loh, G. Li, B. Hu, Z. Liu, H. Gao, X. Chen, Water-responsive supercontractile polymer films for bioelectronic interfaces. *Nature* **624**, 295–302 (2023).
14. Y. Jiang, S. Ji, J. Sun, J. Huang, Y. Li, G. Zou, T. Salim, C. Wang, W. Li, H. Jin, J. Xu, S. Wang, T. Lei, X. Yan, W. Y. X. Peh, S. C. Yen, Z. Liu, M. Yu, H. Zhao, Z. Lu, G. Li, H. Gao, Z. Liu, Z. Bao, X. Chen, A universal interface for plug-and-play assembly of stretchable devices. *Nature* **614**, 456–462 (2023).
15. W. Wang, Y. Jiang, D. Zhong, Z. Zhang, S. Choudhury, J. C. Lai, H. Gong, S. Niu, X. Yan, Y. Zheng, C. C. Shih, R. Ning, Q. Lin, D. Li, Y. H. Kim, J. Kim, Y. X. Wang, C. Zhao, C. Xu, X. Ji, Y. Nishio, H. Lyu, J. B. H. Tok, Z. Bao, Neuromorphic sensorimotor loop embodied by monolithically integrated, low-voltage, soft e-skin. *Science* **380**, 735–742 (2023).
16. W. Zhou, Y. Jiang, Q. Xu, L. Chen, H. Qiao, Y. X. Wang, J. C. Lai, D. Zhong, Y. Zhang, W. Li, Y. du, X. Wang, J. Lei, G. Dong, X. Guan, S. Ma, P. Kang, L. Yuan, M. Zhang, J. B. H. Tok, D. Li, Z. Bao, W. Jia, Soft and stretchable organic bioelectronics for continuous intraoperative neurophysiological monitoring during microsurgery. *Nat. Biomed. Eng.* **7**, 1270–1281 (2023).

17. B. Du, S. Xiong, L. Sun, Y. Tagawa, D. Inoue, D. Hashizume, W. Wang, R. Guo, T. Yokota, S. Wang, Y. Ishida, S. Lee, K. Fukuda, T. Someya, A water-resistant, ultrathin, conformable organic photodetector for vital sign monitoring. *Sci. Adv.* **10**, eadp2679 (2024).
18. D.-H. Kim, N. Lu, R. Ma, Y. S. Kim, R. H. Kim, S. Wang, J. Wu, S. M. Won, H. Tao, A. Islam, K. J. Yu, T. I. Kim, R. Chowdhury, M. Ying, L. Xu, M. Li, H. J. Chung, H. Keum, M. McCormick, P. Liu, Y. W. Zhang, F. G. Omenetto, Y. Huang, T. Coleman, J. A. Rogers, Epidermal electronics. *Science* **333**, 838–843 (2011).
19. S. Xu, Y. Zhang, L. Jia, K. E. Mathewson, K. I. Jang, J. Kim, H. Fu, X. Huang, P. Chava, R. Wang, S. Bhole, L. Wang, Y. J. Na, Y. Guan, M. Flavin, Z. Han, Y. Huang, J. A. Rogers, Soft microfluidic assemblies of sensors, circuits, and radios for the skin. *Science* **344**, 70–74 (2014).
20. H. U. Chung, B. H. Kim, J. Y. Lee, J. Lee, Z. Xie, E. M. Ibler, K. Lee, A. Banks, J. Y. Jeong, J. Kim, C. Ogle, D. Grande, Y. Yu, H. Jang, P. Assem, D. Ryu, J. W. Kwak, M. Namkoong, J. B. Park, Y. Lee, D. H. Kim, A. Ryu, J. Jeong, K. You, B. Ji, Z. Liu, Q. Huo, X. Feng, Y. Deng, Y. Xu, K. I. Jang, Y. Zhang, R. Ghaffari, C. M. Rand, M. Schau, A. Hamvas, D. E. Weese-Mayer, Y. Huang, S. M. Lee, C. H. Lee, N. R. Shanbhag, A. S. Paller, S. Xu, J. A. Rogers, Binodal, wireless epidermal electronic systems with in-sensor analytics for neonatal intensive care. *Science* **363**, eaau0780 (2019).
21. H. U. Chung, A. Y. Rwei, A. Hourlier-Fargette, S. Xu, K. Lee, E. C. Dunne, Z. Xie, C. Liu, A. Carlini, D. H. Kim, D. Ryu, E. Kulikova, J. Cao, I. C. Odland, K. B. Fields, B. Hopkins, A. Banks, C. Ogle, D. Grande, J. B. Park, J. Kim, M. Irie, H. Jang, J. Lee, Y. Park, H. H. Jo, H. Hahm, R. Avila, Y. Xu, M. Namkoong, J. W. Kwak, E. Suen, M. A. Paulus, R. J. Kim, B. V. Parsons, K. A. Human, S. S. Kim, M. Patel, W. Reuther, H. S. Kim, S. H. Lee, J. D. Leedle, Y. Yun, S. Rigali, T. Son, I. Jung, H. Arafa, V. R. Soundararajan, A. Ollech, A. Shukla, A. Bradley, M. Schau, C. M. Rand, L. E. Marsillio, Z. L. Harris, Y. Huang, A. Hamvas, A. S. Paller, D. E. Weese-Mayer, J. Y. Lee, J. A. Rogers, Skin-interfaced biosensors for advanced wireless physiological monitoring in neonatal and pediatric intensive-care units. *Nat. Med.* **26**, 418–429 (2020).
22. K. Kwon, J. U. Kim, S. M. Won, J. Zhao, R. Avila, H. Wang, K. S. Chun, H. Jang, K. H. Lee, J. H. Kim, S. Yoo, Y. J. Kang, J. Kim, J. Lim, Y. Park, W. Lu, T. I. Kim, A. Banks, Y. Huang, J. A. Rogers, A battery-less wireless implant for the continuous monitoring of vascular pressure, flow rate and temperature. *Nat. Biomed. Eng.* **7**, 1215–1228 (2023).
23. W. Gao, S. Emaminejad, H. Y. Y. Nyein, S. Challa, K. Chen, A. Peck, H. M. Fahad, H. Ota, H. Shiraki, D. Kiriya, D.-H. Lien, G. A. Brooks, R. W. Davis, A. Javey, Fully integrated wearable sensor arrays for multiplexed in situ perspiration analysis. *Nature* **529**, 509–514 (2016).
24. J. Tu, J. Min, Y. Song, C. Xu, J. Li, J. Moore, J. Hanson, E. Hu, T. Parimon, T. Y. Wang, E. Davoodi, T. F. Chou, P. Chen, J. J. Hsu, H. B. Rossiter, W. Gao, A wireless patch for the monitoring of C-reactive protein in sweat. *Nat. Biomed. Eng.* **7**, 1293–1306 (2023).
25. B. Zhang, J. Li, J. Zhou, L. Chow, G. Zhao, Y. Huang, Z. Ma, Q. Zhang, Y. Yang, C. K. Yiu, J. Li, F. Chun, X. Huang, Y. Gao, P. Wu, S. Jia, H. Li, D. Li, Y. Liu, K. Yao, R. Shi, Z. Chen, B. L. Khoo, W. Yang, F. Wang, Z. Zheng, Z. Wang, X. Yu, A three-dimensional liquid diode for soft, integrated permeable electronics. *Nature* **628**, 84–92 (2024).
26. C. Chen, S. Ding, J. Wang, Digital health for aging populations. *Nat. Med.* **29**, 1623–1630 (2023).
27. S.-H. Sunwoo, S. I. Han, C. S. Park, J. H. Kim, J. S. Georgiou, S. P. Lee, D. H. Kim, T. Hyeon, Soft bioelectronics for the management of cardiovascular diseases. *Nat. Rev. Bioeng.* **2**, 8–24 (2024).
28. Q. Zheng, Q. Tang, Z. L. Wang, Z. Li, Self-powered cardiovascular electronic devices and systems. *Nat. Rev. Cardiol.* **18**, 7–21 (2021).
29. C. Zhao, J. Park, S. E. Root, Z. Bao, Skin-inspired soft bioelectronic materials, devices and systems. *Nat. Rev. Bioeng.* **2**, 671–690 (2024).
30. S. Lee, X. Liang, J. S. Kim, T. Yokota, K. Fukuda, T. Someya, Permeable bioelectronics toward biointegrated systems. *Chem. Rev.* **124**, 6543–6591 (2024).
31. G. S. Ginsburg, R. W. Picard, S. H. Friend, Key issues as wearable digital health technologies enter clinical care. *N. Engl. J. Med.* **390**, 1118–1127 (2024).
32. K. Bayoumy, M. Gaber, A. Elshafeey, O. Mhaimeed, E. H. Dineen, F. A. Marvel, S. S. Martin, E. D. Muse, M. P. Turakhia, K. G. Tarakji, M. B. Elshazly, Smart wearable devices in cardiovascular care: Where we are and how to move forward. *Nat. Rev. Cardiol.* **18**, 581–599 (2021).
33. J. R. Walter, S. Xu, J. A. Rogers, From lab to life: How wearable devices can improve health equity. *Nat. Commun.* **15**, 123 (2024).
34. A. K. Khanna, J. O. Garcia, A. K. Saha, L. Harris, M. Baruch, R. S. Martin, Agreement between cardiac output estimation with a wireless, wearable pulse decomposition analysis device and continuous thermodilution in post cardiac surgery intensive care unit patients. *J. Clin. Monit. Comput.* **38**, 139–146 (2024).
35. Y. Wu, J. Cheng, J. Qi, C. Hang, R. Dong, B. C. Low, H. Yu, X. Jiang, Three-dimensional liquid metal-based neuro-interfaces for human hippocampal organoids. *Nat. Commun.* **15**, 4047 (2024).
36. K. Nan, S. Babaee, W. W. Chan, J. L. P. Kuosmanen, V. R. Feig, Y. Luo, S. S. Srinivasan, C. M. Patterson, A. M. Jebran, G. Traverso, Low-cost gastrointestinal manometry via silicone–liquid-metal pressure transducers resembling a quipu. *Nat. Biomed. Eng.* **6**, 1092–1104 (2022).
37. J. Yan, Y. Lu, G. Chen, M. Yang, Z. Gu, Advances in liquid metals for biomedical applications. *Chem. Soc. Rev.* **47**, 2518–2533 (2018).
38. Q. Zhuang, K. Yao, M. Wu, Z. Lei, F. Chen, J. Li, Q. Mei, Y. Zhou, Q. Huang, X. Zhao, Y. Li, X. Yu, Z. Zheng, Wafer-patterned, permeable, and stretchable liquid metal microelectrodes for implantable bioelectronics with chronic biocompatibility. *Sci. Adv.* **9**, eadg8602 (2023).
39. T. Daeneke, K. Khoshmanesh, N. Mahmood, I. A. de Castro, D. Esrafilzadeh, S. J. Barrow, M. D. Dickey, K. Kalantar-zadeh, Liquid metals: Fundamentals and applications in chemistry. *Chem. Soc. Rev.* **47**, 4073–4111 (2018).
40. M. Kong, M. H. Vong, M. Kwak, I. Lim, Y. Lee, S. H. Lee, I. You, O. Awartani, J. Kwon, T. J. Shin, U. Jeong, M. D. Dickey, Ambient printing of native oxides for ultrathin transparent flexible circuit boards. *Science* **385**, 731–737 (2024).
41. J. Tang, A. J. Christofferson, J. Sun, Q. Zhai, P. V. Kumar, J. A. Yuwono, M. Tajik, N. Meftahi, J. Tang, L. Dai, G. Mao, S. P. Russo, R. B. Kaner, M. A. Rahim, K. Kalantar-Zadeh, Dynamic configurations of metallic atoms in the liquid state for selective propylene synthesis. *Nat. Nanotechnol.* **19**, 306–310 (2024).
42. W. Lee, H. Kim, I. Kang, H. Park, J. Jung, H. Lee, J. S. Park, J. M. Yuk, S. Ryu, J.-W. Jeong, J. Kang, Universal assembly of liquid metal particles in polymers enables elastic printed circuit board. *Science* **378**, 637–641 (2022).
43. Q. Zhuang, K. Yao, C. Zhang, X. Song, J. Zhou, Y. Zhang, Q. Huang, Y. Zhou, X. Yu, Z. Zheng, Permeable, three-dimensional integrated electronic skins with stretchable hybrid liquid metal solders. *Nat. Electron.* **7**, 598–609 (2024).
44. H. Yuk, C. E. Varela, C. S. Nabzdyk, X. Mao, R. F. Padera, E. T. Roche, X. Zhao, Dry double-sided tape for adhesion of wet tissues and devices. *Nature* **575**, 169–174 (2019).
45. J. Deng, H. Yuk, J. Wu, C. E. Varela, X. Chen, E. T. Roche, C. F. Guo, X. Zhao, Electrical bioadhesive interface for bioelectronics. *Nat. Mater.* **20**, 229–236 (2021).
46. X. Zhang, S. Liu, X. Weng, T. Wu, L. Yu, Y. Xu, J. Guo, Brg1 trans-activates endothelium-derived colony stimulating factor to promote calcium chloride induced abdominal aortic aneurysm in mice. *J. Mol. Cell. Cardiol.* **125**, 6–17 (2018).
47. M. R. Malinow, F. F. Batlle, B. Malamud, Nervous mechanisms in ventricular arrhythmias induced by calcium chloride in rats. *Circ. Res.* **1**, 554–559 (1953).
48. L. Venetucci, M. Denegri, C. Napolitano, S. G. Priori, Inherited calcium channelopathies in the pathophysiology of arrhythmias. *Nat. Rev. Cardiol.* **9**, 561–575 (2012).
49. J. H. Koo, S. Jeong, H. J. Shim, D. Son, J. Kim, D. C. Kim, S. Choi, J. I. Hong, D. H. Kim, Wearable electrocardiogram monitor using carbon nanotube electronics and color-tunable organic light-emitting diodes. *ACS Nano* **11**, 10032–10041 (2017).
50. Z. Huang, Y. Hao, Y. Li, H. Hu, C. Wang, A. Nomoto, T. Pan, Y. Gu, Y. Chen, T. Zhang, W. Li, Y. Lei, N. Kim, L. Zhang, J. W. Ward, A. Maralani, X. Li, M. F. Durstock, A. Pisano, Y. Lin, S. Xu, Three-dimensional integrated stretchable electronics. *Nat. Electron.* **1**, 473–480 (2018).
51. S. P. Lee, G. Ha, D. E. Wright, Y. Ma, E. Sen-Gupta, N. R. Haubrich, P. C. Branche, W. Li, G. L. Huppert, M. Johnson, H. B. Mutlu, K. Li, N. Sheth, J. A. Wright Jr., Y. Huang, M. Mansour, J. A. Rogers, R. Ghaffari, Highly flexible, wearable, and disposable cardiac biosensors for remote and ambulatory monitoring. *NPJ Digit. Med.* **1**, 2 (2018).
52. L. Yin, Y. Wang, J. Zhan, Y. Bai, C. Hou, J. Wu, R. Huang, Y. Huang, Chest-scale self-compensated epidermal electronics for standard 6-precordial-lead ECG. *NPJ Flex. Electron.* **6**, 29 (2022).
53. W. Lu, W. Bai, H. Zhang, C. Xu, A. M. Chiarelli, A. Vázquez-Guardado, Z. Xie, H. Shen, K. Nandoliya, H. Zhao, K. H. Lee, Y. Wu, D. Franklin, R. Avila, S. Xu, A. Rwei, M. Han, K. Kwon, Y. Deng, X. Yu, E. B. Thorp, X. Feng, Y. Huang, J. Forbess, Z. D. Ge, J. A. Rogers, Wireless, implantable catheter-type oximeter designed for cardiac oxygen saturation. *Sci. Adv.* **7**, eabe0579 (2021).
54. H. Jeong, J. Y. Lee, K. H. Lee, Y. J. Kang, J. T. Kim, R. Avila, A. Tzavelis, J. Kim, H. Ryu, S. S. Kwak, J. U. Kim, A. Banks, H. Jang, J. K. Chang, S. Li, C. K. Mummidisetty, Y. Park, S. Nappi, K. S. Chun, Y. J. Lee, K. Kwon, X. Ni, H. U. Chung, H. Luan, J. H. Kim, C. Wu, S. Xu, A. Banks, A. Jayaraman, Y. Huang, J. A. Rogers, Differential cardiopulmonary monitoring system for artifact-canceled physiological tracking of athletes, workers, and COVID-19 patients. *Sci. Adv.* **7**, eabg3092 (2021).
55. M. A. Zahed, M. Sharifuzzaman, H. Yoon, M. Asaduzzaman, D. K. Kim, S. Jeong, G. B. Pradhan, Y. D. Shin, S. H. Yoon, S. Sharma, S. Zhang, J. Y. Park, A nanoporous carbon-MXene heterostructured nanocomposite-based epidermal patch for real-time biopotentials and sweat glucose monitoring. *Adv. Funct. Mater.* **32**, 2208344 (2022).
56. C. Yiu, Y. Liu, C. Zhang, J. Zhou, H. Jia, T. H. Wong, X. Huang, J. Li, K. Yao, M. K. Yau, L. Zhao, H. Li, B. Zhang, W. Park, Y. Zhang, Z. Wang, X. Yu, Soft, stretchable, wireless intelligent three-lead electrocardiograph monitors with feedback functions for warning of potential heart attack. *SmartMat* **3**, 668–684 (2022).
57. M. A. Zahed, D. K. Kim, S. H. Jeong, M. Selim Reza, M. Sharifuzzaman, G. B. Pradhan, H. Song, M. Asaduzzaman, J. Y. Park, Microfluidic-integrated multimodal wearable hybrid patch for wireless and continuous physiological monitoring. *ACS Sens.* **8**, 2960–2974 (2023).

Acknowledgments

Funding: RGC Senior Research Fellow Scheme (SRFS2122-5S04) (to Z.Z.), The Hong Kong Polytechnic University 1-ZVQM (to Z.Z.), The Hong Kong Polytechnic University 1-BBXR (to

Z.Z.), The Hong Kong Polytechnic University 1-CD44 (to Z.Z.), Research Grants Council of the Hong Kong Special Administrative Region 15304823 (to Z.Z.), Research Grants Council of the Hong Kong Special Administrative Region RFS2324-1S03 (to X.Y.), Innovation and Technology Fund of Innovation and Technology Commission GHP/260/22SZ (to Z.Z.), City University of Hong Kong (grant nos. 9667221 and 9678274) (to X.Y.), The Foundation of National Natural Science Foundation of China (NSFC) 61421002, The Foundation of National Natural Science Foundation of China (NSFC) 62122002, and in part, InnoHK Project on Project 2.2—AI-based 3D ultrasound imaging algorithm at Hong Kong Centre for Cerebro-Cardiovascular Health Engineering (COCHE) (to X.Y.). **Author contributions:** Conceptualization: Q. Zhuang, K.Y., Z.Z., and X.Y. Methodology: Q. Zhuang, K.Y., Y.C., H.W., X.S., and Q. Zhang. Investigation: Q. Zhuang, K.Y., Q. Zhang, Y.C., G.Z., S.L., X.Y., and R.Y. Validation: Q. Zhuang, K.Y., X.Y., Y.C., C.Z., and Q. Zhang. Formal analysis: Q. Zhuang, K.Y., X.Y., C.Z., and Q. Zhang. Resources: Z.Z., Q. Zhuang, X.Y., Y.C., H.S., Q.H., and S.L. Data curation: Q. Zhuang, K.Y., C.Z., and Q. Zhang. Visualization: Q. Zhuang, K.Y., X.Y., and C.Z. Software: K.Y. and C.Z. Supervision: Z.Z. and X.Y. Writing—original draft: Q. Zhuang and K.Y. Writing—review and editing: Z.Z., X.Y., and Q. Zhuang. Funding acquisition: Z.Z. and X.Y. Project administration: Z.Z. and X.Y. **Competing interests:** The authors have filed a patent titled "An ICU-grade breathable cardiac electronic skin for health, diagnostics, intraoperative and postoperative monitoring" (US 63/670,192). The filing date was 12 July 2024. The inventors include Q. Zhuang and Z.Z. The authors declare that they have no other competing interests. **Data and materials availability:** All data needed to evaluate the conclusions in the papers are present in the paper and/or the Supplementary Materials.

Submitted 1 November 2024
Accepted 13 February 2025
Published 19 March 2025
10.1126/sciadv.adu3146